Journal of Solid State Chemistry 188 (2012) 38–43

Contents lists available at SciVerse ScienceDirect

Journal of Solid State Chemistry

journal homepage: www.elsevier.com/locate/jssc

Hydrothermal synthesis of lutetium disilicate nanoparticles

Xiaoping Tang [a,b], Yanfeng Gao [a,*], Hongfei Chen [a,b], Hongjie Luo [c,**]

[a] State Key Laboratory of High Performance Ceramics and Superfine Microstructure, Shanghai Institute of Ceramics (SIC), Chinese Academy of Sciences (CAS), 1295 Dingxi, Changning, Shanghai 200050, China
[b] Graduate University of Chinese Academy of Sciences, 19 Yuquanlu, Beijing 100049, China
[c] Shanghai Institute of Ceramics (SIC), Chinese Academy of Sciences (CAS), 1295 Dingxi, Changning, Shanghai 200050, China

ARTICLE INFO

Article history:
Received 15 July 2011
Received in revised form
19 January 2012
Accepted 22 January 2012
Available online 30 January 2012

Keywords:
$Lu_2Si_2O_7$
Hydrothermal synthesis
Thermophysical properties
Hot corrosion

ABSTRACT

A simple, low-cost hydrothermal method was developed to synthesize irregular-and rod-shaped lutetium disilicate ($Lu_2Si_2O_7$) powders with sizes ranging from 71 to 340 nm. The synthesis temperature was 260 °C, which is nearly 1300 °C lower than that required for the solid-state reaction. The results indicated that both the hydrothermal temperature and pH values had great influences on the composition, crystalline phase and morphology of the powders. The formation mechanism, basic thermophysical properties, stability and anticorrosion properties of the $Lu_2Si_2O_7$ powders were also investigated. The obtained powders possessed low thermal conductivity, a suitable thermal expansion coefficient ($3.92–5.17\times10^{-6}$ K^{-1}) with the silicon-based substrate and excellent thermal and structural stability. During hot corrosion testing, the surfaces of the samples appeared to react with the water and molten salt vapors, but no serious failure occurred.

1. Introduction

Silicon-based ceramics are promising candidate materials for use in the hot section components of next-generation gas turbine engines due to their superior strength and durability at high temperatures. A major stumbling block to the application of these materials is their poor durability in high velocity combustion environments that contain high-temperature water vapor and molten alkali salts. At high temperatures, a thin silica film that forms on the surface of silicon-based ceramics can react with water vapor and dissolve in molten alkali salts to form volatile materials, which results in the failure of silicon-based ceramics. An environmental barrier coating (EBC) deposited on silicon-based ceramics helps provide protection [1–4]. Rare earth silicates, such as lutetium disilicate (i.e., $Lu_2Si_2O_7$), are potential candidates as EBC materials due to their low thermal diffusivity, excellent durability in severe environments containing both water vapor and alkali salts at high-temperatures, and desirable chemical and mechanical compatibility with the silicon-based matrix [3,5,6].

Solid-state and sol–gel syntheses are two typical routes for the preparation of lutetium silicates. However, the two methods require either annealing at a high sintering temperature (>1200 °C) or complicated processing parameters, and a pure $Lu_2Si_2O_7$ crystal is difficult to obtain. Furthermore, the produced powders usually possess large particle sizes and a wide size distribution, which hinders the formation of dense coatings [7–12]. Basically, a dense coating is required for the EBCs to obstruct the diffusion of corrosive gases. It is, therefore, necessary to develop an easy, low-cost, and efficient method to produce homogeneously dispersed lutetium silicate powders. In our previous work, nano-sized $Yb_2Si_2O_7$ powders were successfully synthesized at 200 °C via a hydrothermal process. The powders were nearly monodispersed and quite uniform in both shape and size, with a mean diameter of 20 nm [13]. In this article, we introduce a hydrothermal synthesis for the preparation of $Lu_2Si_2O_7$ powders beginning with lutetium nitrate ($Lu(NO_3)_3$) and sodium silicate ($Na_2SiO_3\cdot9H_2O$). Short, rod-like, pure-phase $Lu_2Si_2O_7$ powders with high crystallinity and controllable particle sizes were successfully synthesized at 260 °C. We systematically investigated the processing parameters and tested the thermal and physical properties of the products. To our knowledge, this is the first report of the synthesis of $Lu_2Si_2O_7$ by this method.

In this work, the hot corrosion of $Lu_2Si_2O_7$ in a Na_2CO_3 molten salt (MS) atmosphere at various temperatures was also studied. Na_2CO_3 readily decomposes and is used to study corrosion resistance under strongly basic conditions.

$$Na_2CO_3 \rightarrow Na_2O + CO_2\uparrow(g) \quad (1)$$

This study aims to determine the hot corrosion properties of $Lu_2Si_2O_7$ in an alkaline vapor airflow environment. The results of this study are helpful for selecting candidate materials for use as environmental barrier coatings.

* Corresponding author.
** Corresponding author.
E-mail addresses: yfgao@mail.sic.ac.cn, yfgaosic@gmail.com (Y. Gao).

0022-4596/$ - see front matter © 2012 Elsevier Inc. All rights reserved.
doi:10.1016/j.jssc.2012.01.049

2. Experimental procedure

In a typical synthesis, 0.01 mol Lu_2O_3 was dissolved in 30 mL of dilute nitric acid (2 mol L^{-1}) to produce $Lu(NO_3)_3$ solution, and 0.02 mol $Na_2SiO_3 \cdot 9H_2O$ was dissolved in 50 mL of distilled water. The aqueous solution of Na_2SiO_3 was slowly added to the $Lu(NO_3)_3$ solution with stirring. After homogeneous mixing, the pH was adjusted to a certain value (4, 6, 8 and 10) by adding ammonia. A white emulsion formed after ultrasonication for 10 min. After stirring for more than 4 h, the emulsion was sealed in a 250 mL autoclave liner (additional distilled water was added to reach 80% capacity). The autoclaves were then slowly heated to different temperatures (230, 240, 250 and 260 °C) and held for different lengths of time (4, 6, 8, 10, and 12 h). After the reaction, the autoclave was allowed to cool naturally. The obtained powders were washed with distilled water and absolute alcohol several times before drying at 60 °C for 6 h in an oven.

The powders were granulated with 5wt% PVA solution (powder:PVA solution=9:1, mass ration), and then pressed into plates (Φ=10 mm, d=2 mm) under 10 MPa with unidirectional squash. The prepared plates were then sintered at 1200 °C for 3 h to prepare the specimens for hot corrosion tests. To increase the wettability between the plates and the salt mists, no polishing was performed. The specimens were cleaned by ultrasonication in a sequence of distilled water, acetone and alcohol before testing. Fig. 1 shows the schematic of a home-made system for the corrosion behavior tests. Compressed air flowed through a wash bottle containing deionized water and then entered into a tubular furnace. The sample and 0.05 mol of Na_2CO_3 were placed in two Al_2O_3 ceramic boats with the molten salt placed near the airflow entrance. The exhaust gas was collected by another wash bottle. This design ensures that the airflow that passes over the sample contains both water and molten salt vapors. Corrosive properties were tested at both 900 and 1000 °C for 24 and 48 h.

The crystalline structures of the resulting powders were investigated using X-ray diffraction (XRD, D/max 2550 V, RIKAKU, Tokyo), and the morphologies were characterized by scanning electron microscopy (SEM, JSM-6700 F, JEOL, Tokyo). Simultaneous thermogravimetric and differential thermal analyses (TG-DTA, STA429C, NETZSCH, Germany) were performed in air from 30 to 1400 °C with an annealing rate of 10.0 K min^{-1} to determine the thermal properties of the powders. The thermal diffusion and specific heat of the sample were measured as a function of temperature from room temperature (RT) to 1200 °C using the laser-flash method. The thermal expansion of $Lu_2Si_2O_7$ was measured via the push-rod dilatometer method at temperatures from RT to 1200 °C.

3. Results and discussion

3.1. XRD analysis

Fig. 2 shows the XRD patterns of the samples obtained under different conditions. Overall, higher hydrothermal temperatures, longer reaction times and higher pH values led to greater peak

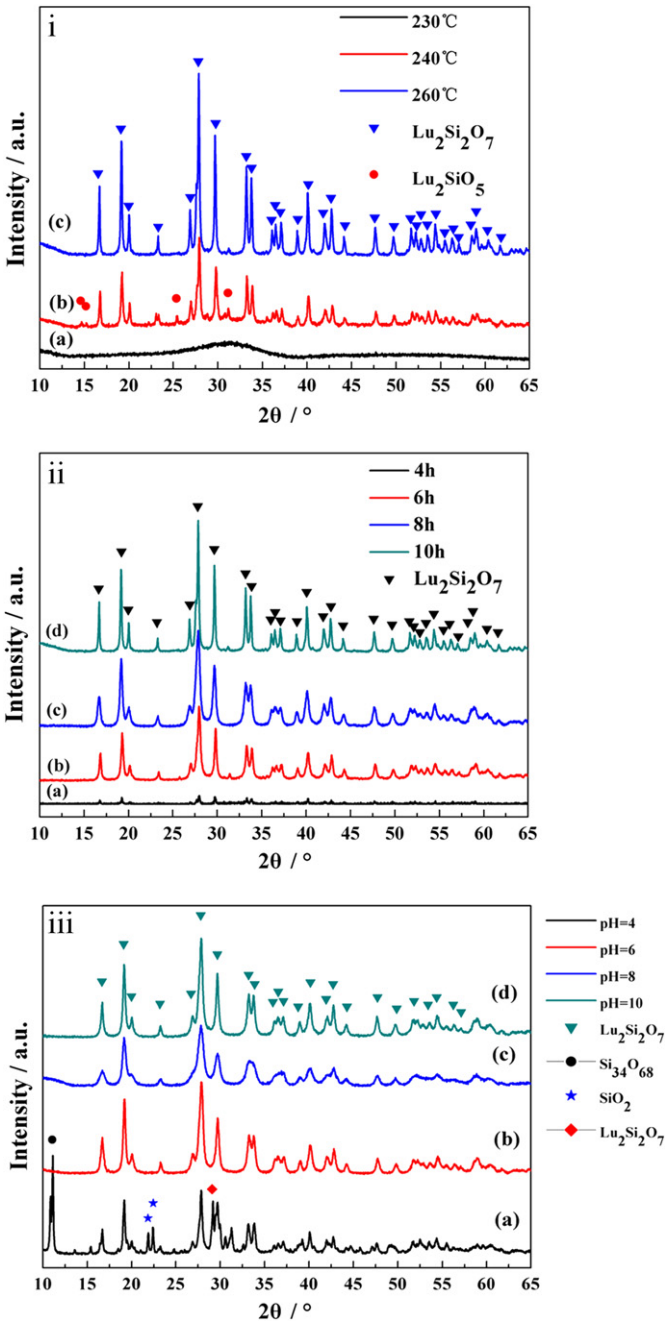

Fig. 2. (i) XRD patterns for powders obtained at different hydration temperatures with the same pH and reaction time (pH=10, 10 h): (a) 230 °C; (b) 240 °C; and (c) 260 °C. Fig.2 (ii) Different hydration times with the same pH and temperature (pH=10, 260 °C): (a) 4 h; (b) 6 h; (c) 8 h; and (d) 10 h. Fig.2 (iii) Different pH values with the same reaction time and temperature (10 h, 260 °C): (a) pH=4; (b) pH=6; (c) pH=8; and (d) pH=10.

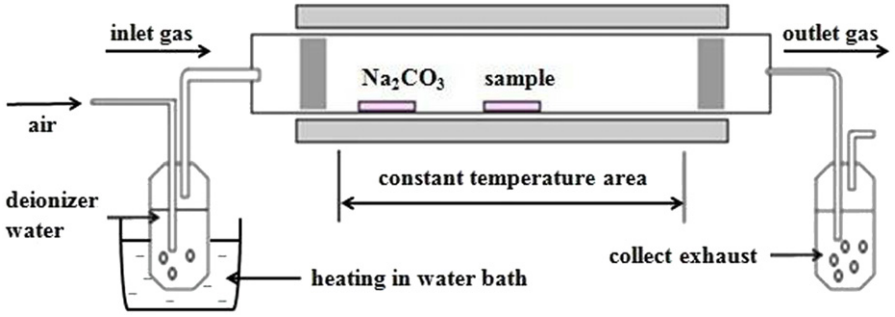

Fig. 1. Schematic drawing of the equipment used for corrosion testing.

intensity, which meant greater crystallinity and larger crystallite sizes. Fig. 2 (i) shows that the product was almost amorphous below 230 °C. At 240 °C, the primary peaks belonged to the monoclinic $Lu_2Si_2O_7$ phase with lattice constants of $a=6.779$ Å, $b=8.848$ Å, $c=4.725$ Å (JCPDS Card No. 35-0326), but a minor phase, Lu_2SiO_5 (JCPDS Card No. 41-0239, $a=12.362$ Å, $b=6.644$ Å, $c=10.252$ Å), was also observed. Upon increasing the temperature to 260 °C, the diffraction peaks for the Lu_2SiO_5 phase disappeared, and the peaks for $Lu_2Si_2O_7$ became sharper. The effects of the hydrothermal reaction time are shown in Fig. 2 (ii). The crystallinity increased with longer reaction times, and no other phases appeared. These results indicated that higher temperatures favor the nucleation and formation of $Lu_2Si_2O_7$ crystals, which is expected to occur through the following reactions:

$$Lu^{3+} + xNO_3^- + (3-x)OH^- \rightarrow Lu(OH)_{(3-x)}(NO_3^-)_x\downarrow \quad (2)$$

$$3NH_4^+ + Lu(OH)_3 + xH_2O \rightarrow (NH_4^+)_3Lu(OH)_6\cdot aq\downarrow \text{ or } (NH_4^+)_4Lu(OH)_7\cdot aq\downarrow \quad (3)$$

$$SiO_3^{2-} + 2H^+ \rightarrow H_2SiO_3\downarrow \quad (4)$$

$$2H_2SiO_3 + 2OH^- \rightarrow Si_2O_5^{2-} + 3H_2O \quad (5)$$

$$Si_2O_5^{2-} + 4OH^- \rightarrow Si_2O_7^{6-} + 3H_2O \quad (6)$$

$$2Lu(OH)_3 + 2H_2SiO_3 \rightarrow Lu_2Si_2O_7 + 5H_2O \quad (7)$$

$$2Lu^{3+} + Si_2O_7^{6-} \rightarrow Lu_2Si_2O_7 \quad (8)$$

$$2(NH_4^+)_3Lu(OH)_6 + 2H_2SiO_3 \rightarrow Lu_2Si_2O_7 + 5H_2O + 6NH_4^+ + 6OH^- \quad (9)$$

As expressed in Eqs. (2)–(4), Lu^{3+} and SiO_3^{2-} ions reacted with OH^- and H^+ to form precipitates during the precursor formation stage and were dependent on the pH value of the precursor solution. The Lu^{3+} and OH^- ions in various solutions at pH ≈ 6 to 8 precipitate as $Lu(OH)_{(3-x)}(NO_3^-)_x$, where $0<x\leq 1$. Aging replaces more, or even all, of the NO_3^- with OH^-. At higher pH values, the precipitate would be slightly dissolved, and $(NH_4^+)_3Lu(OH)_6\cdot aq$ or $(NH_4^+)_4Lu(OH)_7\cdot aq$ can be generated [14]. The next steps (7–9) were occurred in the hydrothermal stage to form ultimate product $Lu_2Si_2O_7$. It was considered that the three reactions were coexisted, and which was the dominant one depended on the precursor aging time and pH value. The XRD results of the samples obtained with different pH values are shown in Fig. 2 (iii). Under acidic conditions (pH=4), SiO_2 (JCPDS Card No.51-1379, $a=12.843$ Å, $b=12.843$ Å, $c=25.196$ Å), $Si_{34}O_{68}$ (JCPDS Card No.52-0144, $a=13.175$ Å, $b=13.175$ Å, $c=15.848$ Å) and $Lu_2Si_2O_7$ (JCPDS Card No.31-0778, $a=5.494$ Å, $b=10.660$ Å, $c=4.688$ Å) formed along with the monoclinic $Lu_2Si_2O_7$ phase (JCPDS Card No. 35-0326). The formation of silicon oxide was due to the high H^+ concentration in the solution. According to Eq. (4), a mass of H_2SiO_3 was formed at first. Due to the suppression of Eqs. (2) and (3), inadequate quantity of $Lu(OH)_3$ precipitated in the precursor. Besides, OH^- was also not enough to stimulate Eqs. (5) and (6), which resulted in the decomposition and independent nucleation of a small quantity of H_2SiO_3 to form silicon oxide during the initial stages of the hydrothermal process, as shown in Eq. (10).

$$H_2SiO_3 \rightarrow SiO_2 + H_2O \quad (10)$$

As the reactions progressed, the H^+ was consumed and the concentration of OH^- increased, then Eqs. (5)–(6) were initiated, resulted in the $Lu_2Si_2O_7$ phase (JCPDS Card No. 35-0326) obtaining. Solution pH values also affected the charge properties and coordination of the ions in the solution. This can explain the formation of allotropic $Lu_2Si_2O_7$ (JCPDS Card No.31-0778) was also formed. At higher pH ($pH\geq 6$), the pure $Lu_2Si_2O_7$ phase formed for the reason there was sufficient OH^- to combine with the Lu^{3+} ions and formed the precipitates in the precursor, indicating that Eqs. (2),(3),(5) and (6) were all accelerated. Eqs. (7) and (9) may be the two primary reactions in the hydrothermal process under such conditions.

3.2. SEM observation

The morphology of the $Lu_2Si_2O_7$ powders obtained under different conditions was characterized by SEM (Fig. 3). The particles obtained upon hydrothermal treatment for 10 h at a pH of 10 and a temperature of 240 or 260 °C were either irregular with a wide size-distribution (Fig. 3(a)) or rod-shaped (Fig. 3(f)), respectively. For samples heated at 260 °C with a pH of 10 (Fig. 3 (b), (c), (f)), prolonging the reaction time resulted in an increase in particle size and the transition of the particle morphology from spherical (Fig. 3(b)) to rod shape (Fig. 3(f)). After reacting for 4 h, the products mainly consisted of spherical nanoparticles that had

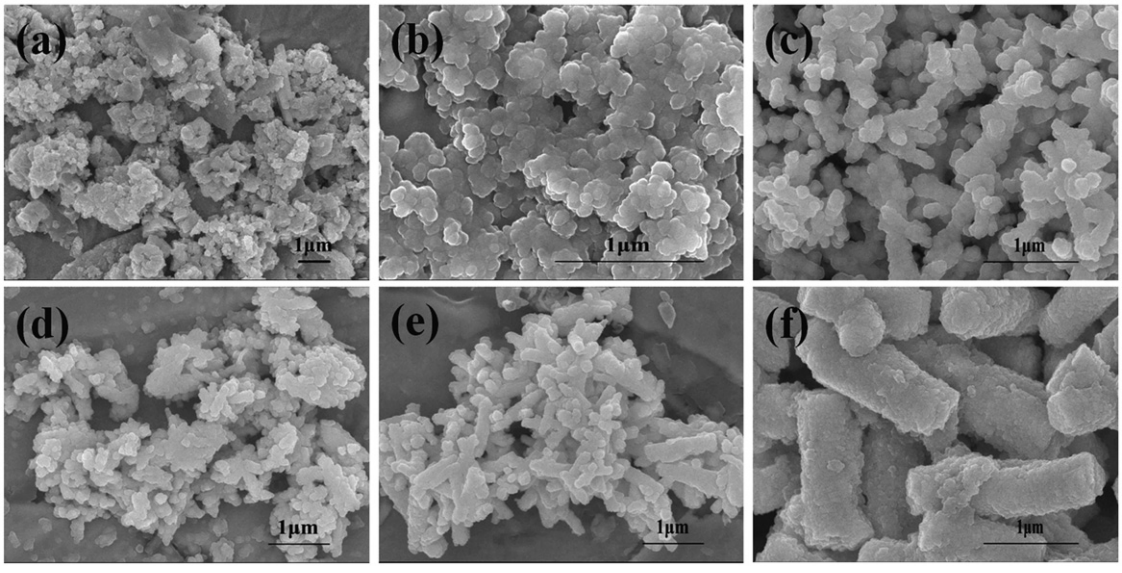

Fig. 3. SEM images of powders produced under different conditions: (a) $T=240$ °C, $t=10$ h, pH=10; (b) $T=260$ °C, $t=4$ h, pH=10; (c) $T=260$ °C, $t=8$ h, pH=10; (d) $T=260$ °C, $t=10$ h, pH=4; (e) $T=260$ °C, $t=10$ h, pH=8; and (f) $T=260$ °C, $t=10$ h, pH=10.

aggregated. Prolonging the reaction time to 8 h caused short, rod-shaped particles with an average diameter of 210 nm to appear. After 10 h, rods with an average length of 1460 nm and a diameter of 340 nm were observed. According to the above results, the Ostwald Ripening (OR) mechanism was primarily responsible for the growth of the rod structures. Upon the extension of the reaction time, the smaller particles dissolved and were redeposited onto the surface of the larger particles. The crystal structure of $Lu_2Si_2O_7$ is thortveitite, which can be described as a close hexagonal packing of the oxygen atoms with Lu^{3+} cations in the octahedral vacancies and Si^{4+} in the tetrahedral vacancies in alternating parallel layers (0 0 1) [15]. The rods formed as a result of the recrystallization process occurring along a certain orientation.

The effects of the pH value on the morphologies are shown in Fig. 3 (d)–(f). At the lower pH value, most particles were irregular, just as in Fig. 3(a), but there were still some rod-shaped particles. The transition to obviously rod-shaped particles was observed as the pH value increased, which shows that, at the same reaction temperature and time, higher pH values (pH > 4) favor the formation of the rod-shaped morphology. In addition, the rods became larger as the pH value increased. Under acidic conditions, Lu^{3+} was difficult to precipitate, and the reaction was inclined to form a silicon oxide nucleus first, and then form $Lu_2Si_2O_7$. Besides, at the condition with pH=4, the existing of impurities may also affected the morphology of particles. In addition, the positive surface potential made it harder for the particles to bond with each other. However, at higher pH, there was a sufficient concentration of OH^- to accelerate the formation of $Lu_2Si_2O_7$, which resulted in easier nucleation and growth. The morphologies and sizes of the powders obtained under different conditions are summarized in Table 1.

3.3. Thermophysical analysis

The TG-DTA results for the sample prepared by heating to 260 °C with a pH of 10 for 10 h are shown in Fig. 4(i). As the temperature increased, the weight loss continued without any obvious exothermic or endothermic peaks, and after 800 °C, the weight loss became more gradual. The weight loss was mainly due to the desorption of water and other volatile impurities which had been introduced during either washing or some other process. No phase transformation or decomposition occurred, according to the TG-DTA, and a sintering experiment was designed to confirm this. Powder obtained under the same conditions was annealed at 1400 °C for 10 min by heating from RT to 1400 °C at a rate of 10.0 K min^{-1} (to simulate the TG-DTA testing), and the results are shown in Fig. 4(ii). No variation occurred after sintering because all of the peaks belonged to the monoclinic $Lu_2Si_2O_7$, just as here. These results demonstrate that $Lu_2Si_2O_7$ powders possess both thermal and structural stability under such conditions.

The thermal diffusivity of $Lu_2Si_2O_7$ decreased upon heating from RT to 1200 °C (Fig. 5), suggesting dominant phonon conduction, which can be found in most polycrystalline materials. The graph of the specific heat (Fig. 6 inset) can be used to extrapolate higher temperature data using the following formula:

$$C_p = 0.39463 + 6.18969E{-}4 \times T - 2.37338E{-}7 \times T^2 R = 0.99999 \quad (11)$$

where C_p is the specific heat (J g^{-1} K^{-1}), T is the testing temperature (°C) and R is the reliability value.

Values for the thermal conductivity are then obtained by multiplying the thermal diffusivity (α), density (ρ) and specific heat (C_p) according to formula (12), where the density of $Lu_2Si_2O_7$ is 6.08 g cm^{-3} when measured by the Archimedes method.

$$\kappa = C_p \cdot \alpha \cdot \rho \quad (12)$$

Table 1
Morphologies and sizes of powders obtained under different conditions.

No.	Temperature (°C)	Time (h)	pH	Morphology	Size (nm)	
					Radial	Axial
1	240	10	10	Irregular	–	
2	260	4	10	Particulate	71	
3	260	8	10	Rod	201	840
4	260	10	4	Irregular	–	
5	260	10	8	Rod + particulate	175	916
6	260	10	10	Rod	340	1460

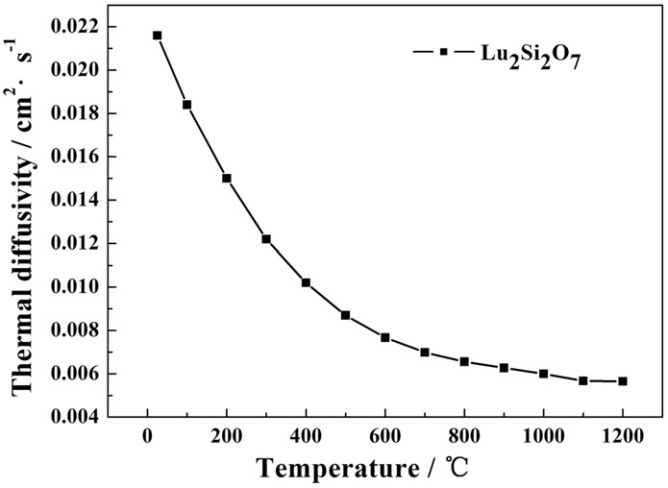

Fig. 5. Thermal diffusivity of $Lu_2Si_2O_7$ powders prepared at 260 °C for 10 h, pH=10.

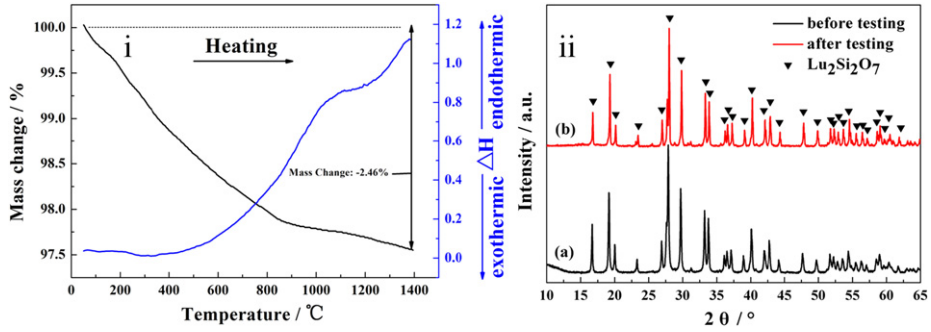

Fig. 4. (i) TG-DTA traces of the sample prepared at 260 °C, pH=10 for 10 h; (ii) XRD patterns of the sample (a) before and (b) after testing.

The calculated values for the thermal conductivity are shown in Fig. 6. While the thermal diffusivity decreases in the temperature range between 1100 and 1200 °C, the thermal conductivity increases, which is attributed to the effect of thermal radiation.

The silicon-based ceramics used in turbines have a coefficient of thermal expansion (CTE) from 3.7 to $5.1\times10^{-6}\,K^{-1}$ ($3.7\times10^{-6}\,K^{-1}$ for Si_3N_4, $4.7\times10^{-6}\,K^{-1}$ for α-SiC and $5.1\times10^{-6}\,K^{-1}$ for β-SiC) [16]. As shown in Fig. 7, the CTE of $Lu_2Si_2O_7$ continued to rise with the temperature to a value of $5.17\times10^{-6}\,K^{-1}$ before dropping to $3.92\times10^{-6}\,K^{-1}$. Very similar CTE values at high temperatures between $Lu_2Si_2O_7$ and the ceramic substrates guarantee low thermal stress at the coating and substrate interface under usage conditions. Thereby, it can be speculated that $Lu_2Si_2O_7$ coating would have good thermal cycling resistance.

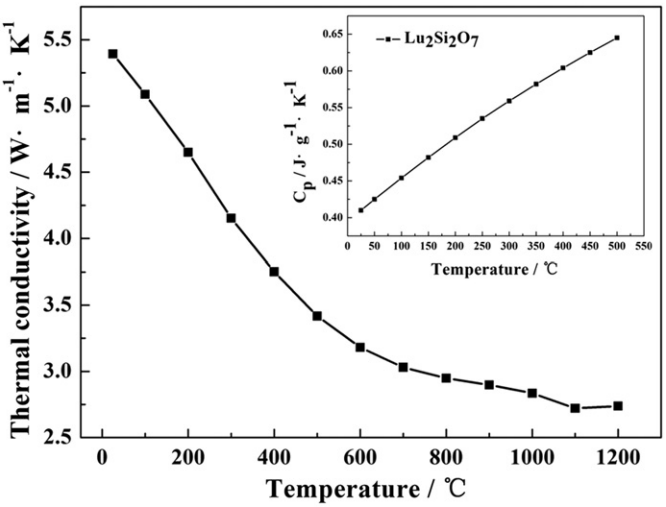

Fig. 6. Temperature dependence of the thermal conductivity and specific heat (insert) of $Lu_2Si_2O_7$.

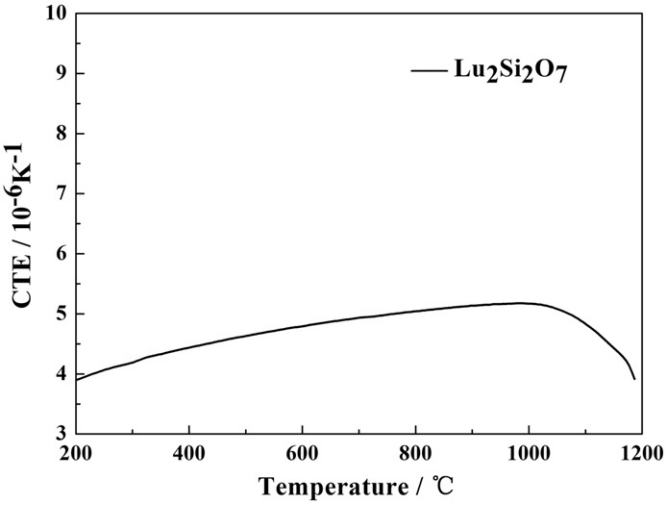

Fig. 7. Thermal expansion coefficients of $Lu_2Si_2O_7$ prepared at 260 °C for 10 h, pH=10.

3.4. Hot corrosion resistance

After washing in deionized water to remove the residual salt, the surface phase compositions of the wafers both before and after corrosion were investigated by XRD, and the results are shown in Fig. 8. It could be seen that, according to the powder composition, only the $Lu_2Si_2O_7$ phase (JCPDS Card No. 35-0326) was present before the corrosion test. The dominant impurity for the samples corroded at 1000 °C was Lu_2SiO_5 (JCPDS Card No. 41-0239), whereas $NaLuSiO_7$ (JCPDS Card No. 27-0727, $a=5.111$ Å, $b=10.989$ Å, $c=6.417$ Å) was detected at 900 °C. The impurity peaks became sharper with longer corrosion times.

Because the Na_2CO_3 was completely transformed to Na_2O and CO_2, and there was water contained in the atmosphere, the hot corrosion of $Lu_2Si_2O_7$ can be assumed to have been induced by the strongly alkali NaOH.

At high temperatures, $Lu_2Si_2O_7$ spontaneously reacted with H_2O and decomposed to Lu_2SiO_5 and $Si(OH)_4$ (Eq. (13)). [3,10,17–18] NaOH is attracted to $Si(OH)_4$ and then forms a water-soluble material, accelerating the corrosion process [19]. Based on the XRD results for the specimens corroded at 1000 °C, we can speculate that the corrosion pathways are as follows:

$$Lu_2Si_2O_7+H_2O\rightarrow Lu_2SiO_5+Si(OH)_4 \quad (13)$$

$$NaOH+xSi(OH)_4\rightarrow Na_2O\cdot xSiO_2+(2x+1)H_2O \quad (14)$$

In the 900 °C corroded specimens, $NaLuSiO_4$ occurred due to the follow reaction:

$$NaOH+Lu_2Si_2O_7\rightarrow 2NaLuSiO_4+H_2O \quad (15)$$

This result was coordinated with the one obtained by Ziqi Sun et al. They have observed $NaYSiO_4$ produced at 850 and 900 °C in the alkali corroded $Y_2Si_2O_7$ samples [4]. We conjectured that the $NaLuSiO_4$ did not exist in the specimens corroded at 1000 °C, probably because it was unstable at this temperature, decomposing into Lu_2SiO_5 and Na_2SiO_3 as per the formula (16). More experiments are under the way to obtain more details.

$$NaLuSiO_4\rightarrow Lu_2SiO_5+Na_2CO_3 \quad (16)$$

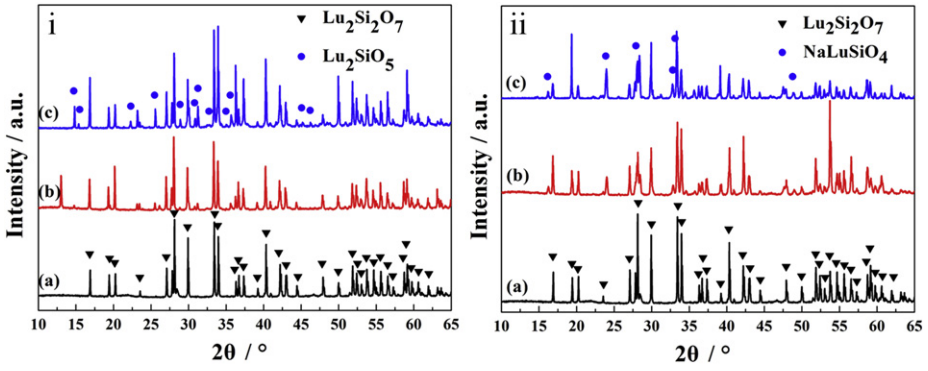

Fig. 8. XRD patterns of as-corroded surfaces of samples under different conditions: (i-a), (ii-a) uncorroded; (i-b) 1000 °C, 24 h; (i-c) 1000 °C, 48 h; (ii-b) 900 °C, 24 h; and (ii-c) 900 °C, 48 h.

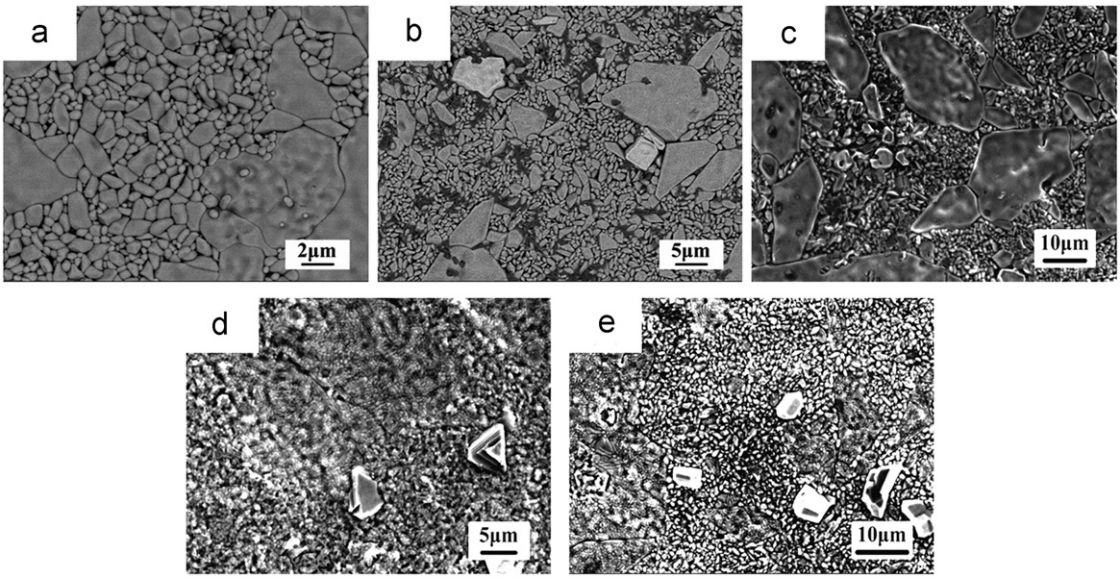

Fig. 9. SEM images of samples surfaces corroded under different conditions: (a) uncorroded; (b) 1000 °C, 24 h; 1000 °C, 48 h; (d) 900 °C, 24 h; (e) 900 °C, 48 h.

The surface morphologies of the samples corroded under different conditions are shown in Fig. 9. The surfaces of the specimens after corrosion were similar to that of the uncorroded specimen. After having been corroded at 1000 °C, the surface grains further grow and bond with each other. While corrosion still occurred at 900 °C, the grain growth was not as obvious, although some small particles still occurred, which may be due to the segregation and re-crystallization of some elements at the surface active sites. There was no serious destruction of the surface structures in any of the samples, which proves that the corrosion only occurs on the surface and that $Lu_2Si_2O_7$ shows excellent stability under testing environments. Further hot corrosion properties are being tested.

4. Conclusions

In this letter, single-crystalline $Lu_2Si_2O_7$ particles were synthesized using a hydrothermal method and the influence of various factors was investigated. The synthesis temperature and the pH value greatly influence the composition, crystallinity and morphology of the products. $Lu_2Si_2O_7$ shows excellent heat insulation and desirable thermal and structural stability. In addition, the hot corrosion experiments demonstrated that it is stable under the conditions tested. All of the results indicate that $Lu_2Si_2O_7$ might be an excellent candidate for use as EBCs.

Acknowledgments

This work is supported in part by the Century Program (One-Hundred-Talent Program), YYYJ-0810 of CAS, NSFC (50972156) and Shanghai Nanoproject (1052nm02100).

References

[1] Kang N. Lee, Robert A. Miller, J. Am. Ceram. Soc. 79 (3) (1996) 620–626.
[2] Kang N. Lee, Dennis S. Fox, Narottam P. Bandsal, J. Eur. Ceram. Soc. 25 (2005) 1705–1715.
[3] Shunkichi Ueno, Tatsuki Ohji, Hua-Tay Lin, J. Ceram. Process Res. 7 (2006) 20–23.
[4] Ziqi Sun, Meishuan Li, Zhongping Li, Qi Sun, Meishuan Li, Zhongping Li, Yanchun Zhou, J. Eur. Ceram. Soc. 28 (2008) 259–265.
[5] Sandeep R. Shah, Rishi Raj, J. Am. Ceram. Soc. 90 (2) (2007) 516–522.
[6] Ziqi Sun, Yanchun Zhou, Jingyang Wang, Meishuan Li, J. Am. Ceram. Soc. 91 (2008) 2623–2629.
[7] D. Doni Jayaseelan, S. Ueno, T. Ohji, S. Kanzaki, Mater. Chem. Phy. 84 (2004) 192–195.
[8] Himansu S. Tripathi, Vinod K. Sarin, Mater. Res. Bull. 42 (2007) 197–202.
[9] N. Maier, G. Rixecker, K.G. Nickel, J. Solid State Chem. 179 (2006) 1630–1635.
[10] Shunkichi Ueno, D. Doni Jayaseelan, Tatsuki Ohji, Hua-Tay Lin, Ceram. Int. 32 (2006) 775–778.
[11] Yong Li, Baogui You, Weiping Zhang, Min Yin, J. Rare Earths 26 (2008) 455–458.
[12] J. Legendiziewicz, J. Sokolnicki, J. Alloys Compd. 451 (2008) 600–605.
[13] Hongfei Chen, Yanfeng Gao, Yun Liu, Hongjie Luo, Inorg. Chem. 49 (2010) 1942–1946.
[14] Ronald L. Rich, Inorganic Reactions in Water, 1st edn., Springer-Verlag, Berlin Heidelberg, 2007.
[15] Youjin Zhang, Hangmin Guan, J. Cryst. Growth 256 (2003) 156–161.
[16] María D. Alba, Pablo Chaín, Appl. Geochem. 22 (2007) 192–201.
[17] S Ueno, D.D. Jayaseelan, T. Ohji, N. Kondo, S. Kanzaki, J. Ceram. Process Res. 4 (2003) 214–216.
[18] N. Maier, K.G Nickel, Georg Rixecker, Key Eng. Mater. 336 (2007) 1780–1783.
[19] Shunkiehi Ueno, Tatsuki Ohji, Hua-Tay Lin, J. Ceram. Process Res. 3 (2006) 201–205.